International Journal of Pharmaceutics 404 (2011) 180–190

Contents lists available at ScienceDirect

International Journal of Pharmaceutics

journal homepage: www.elsevier.com/locate/ijpharm

Pharmaceutical Nanotechnology

Tumor selectivity of stealth multi-functionalized superparamagnetic iron oxide nanoparticles

Caixia Fan[a,b], Wenhui Gao[a], Zhixi Chen[c], Hongyan Fan[d], Mingyan Li[e], Fengjun Deng[f], Zhiliang Chen[a,*]

[a] Department of Pharmacy, Nanfang Hospital, Southern Medical University, Guangzhou, Guangdong, 510515, PR China
[b] Department of Pharmacy, Yuebei People's Hospital, Shaoguan, Guangdong 512026, PR China
[c] Department of Otolaryngology – Head and Neck Surgery, Yuebei People's Hospital, Shaoguan, Guangdong 512026, PR China
[d] Department of Stomatology, Affiliated Hospital, Xiangnan University, Chenzhou, Hunan 423000, PR China
[e] Department of Cardiology, Nanfang Hospital, Southern Medical University, Guangzhou, Guangdong 510515, PR China
[f] Department of Pharmacy, Yiyang Medical College, Yiyang, Hunan 413052, PR China

ARTICLE INFO

Article history:
Received 2 March 2010
Received in revised form 18 October 2010
Accepted 19 October 2010
Available online 16 November 2010

Keywords:
Folic acid
o-Carboxymethylchitosan
Superparamagnetic iron oxide nanoparticles
Tumor targeting

ABSTRACT

Superparamagnetic iron oxide nanoparticles (SPIO-NPs) have traditionally been used as MRI contrast agent for disease imaging via passive targeting. However, there has been an increasing interest in the development of SPIO-NPs to cellular-specific targeting for imaging and drug delivery currently. The objective of our study was to develop a novel active tumor-targeting SPIO-NPs system by surface-modifying superparamagnetic iron oxide nanoparticles (SPIO-NPs) with *o*-carboxymethyl chitosans (OCMCS) and folic acid (FA) to improve their biocompatibility and ability to target specific tumor cells as well as to evade reticuloendothelial system (RES). The results *in vitro* indicated the covalent surface-modification of SPIO-NPs with OCMCS significantly reduced not only the nano-cytotoxicity but also the capture of SPIO-NPs by macrophage cells. On the other hand, the folic acid modification promoted the uptake of nanoparticles by FR-positive tumor cell lines, but had little impact on other cells without folate receptor (FR). MRI image and tumor histological analysis demonstrated the FA-OCMCS-SPIO-NPs had the ability to target tumor cells with FR *in vivo*. OCMCS and folic acid modification of SPIO-NPs could significantly improve both the SPIO-NPs biocompatibility and the FR target for MRI imaging, potential carrier for drug targeting and hyperthermia.

1. Introduction

Superparamagnetic iron oxide nanoparticles (SPIO-NPs) with appropriate surface chemistry have been utilized for magnetic resonance imaging (MRI) (Corot et al., 2006) by passive targeting for several decade years *in vivo*, currently, more and more attention has been paid to developing the second generation of SPIO-NPs targeted to specific cells for MRI (Sun et al., 2008), tissue repair (Heymer et al., 2008), targeted drug delivery (Veiseh et al., 2010) and hyperthermia (Ito et al., 2005). However, the common challenge among these applications is to insure sufficient uptake of SPIO-NPs by specific cells. In order to resolve the problem, the following factors must be taken into account: (a) instability during the storage; (b) a short blood half-life of the SPIO-NPs; (c) nonspecific targeting and (d) low efficiency of internalization (Stella et al., 2000). Bare SPIO-NPs generally have hydrophobic surfaces with a large surface area to volume ratio. This property increases the chance to agglomerate *in vitro* and bind plasma proteins *in vivo*, which result in their instability and very rapid clearance from the circulation by RES (Gupta and Gupta, 2005). Surface modification of these nanoparticles with hydrophilic materials such as derivatives of dextran, polyethylene glycol (PEG), polyethylene oxide (PEO), poloxamers, and polyoxamines, has been widely explored to solve the abovementioned problem. Furthermore, the mean hydrophilic size should be controlled in 10–100 nm to escape rapid renal clearance and capture by the reticuloendothelial system (RES) (Gupta and Gupta, 2005; Shubayev et al., 2009).

Chitosan, obtained by the deacetylation of chitin, has been widely applied in tissue engineering, controlled drug/gene delivery (Katas and Alpar, 2006) because of its abundant availability, biocompatibility, biodegradability, non-toxicity, low-immunogenicity and the possession of the primary amine groups located on the backbone renders chitosan positively charged (Agnihotri et al., 2004). However, the solubility of chitosan is limited to moderately acid aqueous media, and thus it poses a formidable challenge to

* Corresponding author. Tel.: +86 13609786688; mobile: +86 20 61642181.
E-mail address: mydream0509@yahoo.com.cn (Z. Chen).

0378-5173/$ – see front matter © 2010 Elsevier B.V. All rights reserved.
doi:10.1016/j.ijpharm.2010.10.038

many of its potential applications. OCMCS is a water-soluble chitosan derivative, in which the original *o*-hydroxyl group of each monomer is substituted by carboxymethyl group through ether bond. Consequently, the carboxyl groups and amino groups in OCMCS significantly improve its solubility and physicochemical properties including the antimicrobial activity, film-formation and interactions with different substances. Therefore, the OCMCS can be applied in some fields where chitosan has been limited to apply due to its restricted solubility or no suitable functional groups (Zhu et al., 2007; Elsabee et al., 2009). Of note, the OCMCS can stabilize superparamagnetic iron oxide nanoparticles via covalent or non-covalent surface modification (Zhou et al., 2006; Zhu et al., 2008). However, few investigations have been directed to the *in vivo* application of such OCMCS-modified superparamagnetic iron oxide nanoparticles.

In order to increase the local accumulation and retention of the SPIO-NPs in pathological sites while to reduce their side effects, the surface of the SPIO-NPs are usually modified with a ligand such as peptides, aptamers, and small biomolecules with high affinity (Veiseh et al., 2010). FR is a high-affinity glycosylphosphatidylinositol-anchor, which is only expressed in measurable quantities on the surface of most cancer cells, activated macrophages, placenta, and the apical surfaces of some polarized epithelia, while, the FR is generally absent in most normal tissues. Thus, FR provides a highly selective marker that can distinguish tumor cells from normal cells (Reddy and Low, 1998; Sudimack and Lee, 2000; Leamon and Low, 2001; Low and Antony, 2004; Parker et al., 2005). Moreover, FR can cycle in the process of the FR-mediated endocytosis, which supplies enough receptors on the surface of tumor cells to bind to more folic acid (Low and Antony, 2004). On the other hand, folic acid is low intrinsic toxic, nonimmunogenic, inexpensive and stable, and the chemical conjugation methods to a variety of therapeutic drugs and imaging agents have already been well developed. (Zhang et al., 2002; Choi et al., 2004; Sun et al., 2006; Chen et al., 2008) Moreover, any macromolecule covalently conjugated to folic acid could be internalized into FR-bearing cells in the same pathway as free folic acid (Low and Antony, 2004). Hence, it is a highly desirable strategy for us to modify the nanoparticle surface with folic acid to target specific cancer cells or tissues via FR-mediated endocytosis for achieving enhanced efficacy and reducing undesired side effects. Based on the perfect physicochemical properties of OCMCS and folic acid, the over-expression of FR on the surface of most tumor cells and their ability to facilitate internalization of polymeric particles via FR-mediated endocytosis, we developed a novel active tumor-targeting SPIO-NPs system by conjugating the SPIO-NPs with OCMCS and folic acid in order.

In this study, we prepared the FA-OCMCS-SPIO-NPs by three steps and the Fourier transform infrared spectroscopy, X-ray diffraction were used to confirm their synthesis, meanwhile, transmission electron microscope (TEM), dynamic light scattering (DLS), zeta-potential measurement and vibrating sample magnetometry (VSM) was applied to characterize their physical property. MTT assay was used to evaluate the cytotoxicity of nanoparticles (uncoated-SPIO-NPs, OCMCS-SPIO-NPs, FA-OCMCS-SPIO-NPs and dextran-SPIO-NPs) against LO2, A549 and KB cell lines. The uptake of the surface-modified nanoparticles by mouse macrophage and three cancer cell lines with different FR expression were visualized using Prussian blue staining and quantified by ferrozine assay to evaluate their ability to evade the RES capture and FR targeting efficiency *in vitro*. FR-targeting *in vivo* was evaluated by comparing the difference of the MRI signal intensity and histology of the tissues between two subcutaneous tumor xenografts grown from implanted KB cells or A549 cells before and after administration of FA-OCMCS-SPIO-NPs or OCMCS-SPIO-NPs.

2. Materials and methods

2.1. Materials

Dextran (molecular weight of 35,000–45,000), carbodiimide, SephacryS-300HR gel which was produced by the U.S. Pharmacia, folic acid(FA), N-hydroxysuccinimide (NHS), dicyclohexylcarbodiimide (DCC), Ferrous ethylenediammonium sulfate, anhydrous dimethyl sulfoxide (DMSO), methylthiazolyldiphenyl-tetrazolium bromide (MTT), ferrozine, neocuproine and ascorbic acid were purchased from Sigma–Aldrich (China (mainland)). Free folic RPMI-1640 medium, RPMI-1640 medium, GIBCO fetal bovine serum, high glucose DMEM medium were purchased from Invitrogen-Life technologies.Phosphate buffered saline (PBS, pH 7.4), penicillin–streptomycin solution, trypsin–EDTA solution and dialysis bags (molecular weight retention 8000–15,000) were purchased from poly-Bio-Technology Co. Ltd.; GMEGA MSCROP ultrafiltration centrifuge tube (MWCO 30 k) were purchased from Yuwei Biology-Technology Co. Ltd. in Guangzhou; *o*-carboxymethyl chitosan (MW 1–2 million, deacetylation degree $\geq$93%, carboxyl group to replace the degree of $\geq$87%) was purchased from Zhejiang Sendai Chitosan Co. Ltd., Ferric chloride ($FeCl_3{\cdot}6H_2O$) ferrous sulfate ($FeSO_4{\cdot}7H_2O$), $KMnO_4$, concentrated hydrochloric acid(28% $NH_4{\cdot}OH$ in water solution), ammonium acetate, sodium dihydrogen phosphate, disodium hydrogen phosphate, potassium ferrocyanide (II) trihydrate, triethylamine and 95% of ethanol were purchased from Guangzhou chemical reagent Co. Ltd., and all reagent were AR grade. The ultra-pure water was used during the whole study.

2.2. Preparation of the FA-OCMCS-SPIO-NPs and dextran-SPIO-NPs

2.2.1. Preparation of the FA-OCMCS-SPIO-NPs

The preparing process of FA-OCMCS-SPIO-NPs was illustrated schematically in Fig. 1. A brief description of the procedure was as follows: Firstly, SPIO-NPs of approximately 10 nm diameter were prepared by alkaline co-precipitation of ferric chlorides ($FeC1_3{\cdot}6H_2O$) and ferrous sulfate ($FeSO_4{\cdot}7H_2O$) with molar ratio of 2:1 according to the method previously described (Gnanaprakash et al., 2007). The black precipitates were isolated by applying a permanent magnet, washed three times with ultra-pure water to a neutral pH and vacuum dried. There are –OH groups on the surface of the SPIO-NPs when dispersed in water solution, and these surface OH groups were utilized to covalently bind OCMCS to prepare OCMCS-SPIO-NPs (Zhou et al., 2006). Secondly, 200 mg SPIO-NPs were dispersed in 20 ml of deoxygenated carbodiimide buffer A (0.003 mol L^{-1} phosphate buffer containing 1 mol L^{-1} NaCl solution and 6 mg mL^{-1} carbodiimide solution, pH = 6) by sonication (600 W, 10 min). To this solution, 30 ml of OCMCS solution (40 g L^{-1} in buffer A) was added, then, the reaction was continued for 60 min. The synthesized OCMCS-SPIO-NPs were then purified in sequence by centrifuge (3000 rpm) for 30 min, gel filtration chromatography (Sephacryl S-300-HR; Sigma–Aldrich) and dialysis for 24 h using 12 kD cut off dialysis membrane against ultra pure water, and concentrated by a ultrafiltration centrifuge tube (MWCO 30 k). Then, the resulting product was washed with ultra pure water and ethanol three times each and stored at 4 °C for subsequent functionalization with folic acid. Folic acid is generally difficult to conjugate to the surface of the polymer because of the weak chemical reactivity of the carboxylic acid group. Thus, carboxyl group of folic acid was first activated with dicyclohexyl carbodiimide (DCC) and N-hydroxysuccinimide (NHS) to synthesize the NHS-folate according to the method previously described (Choi et al., 2004); at the same time, OCMCS-SPIO-NPs were washed three times with anhydrous DMSO and dispersed in anhydrous DMSO by

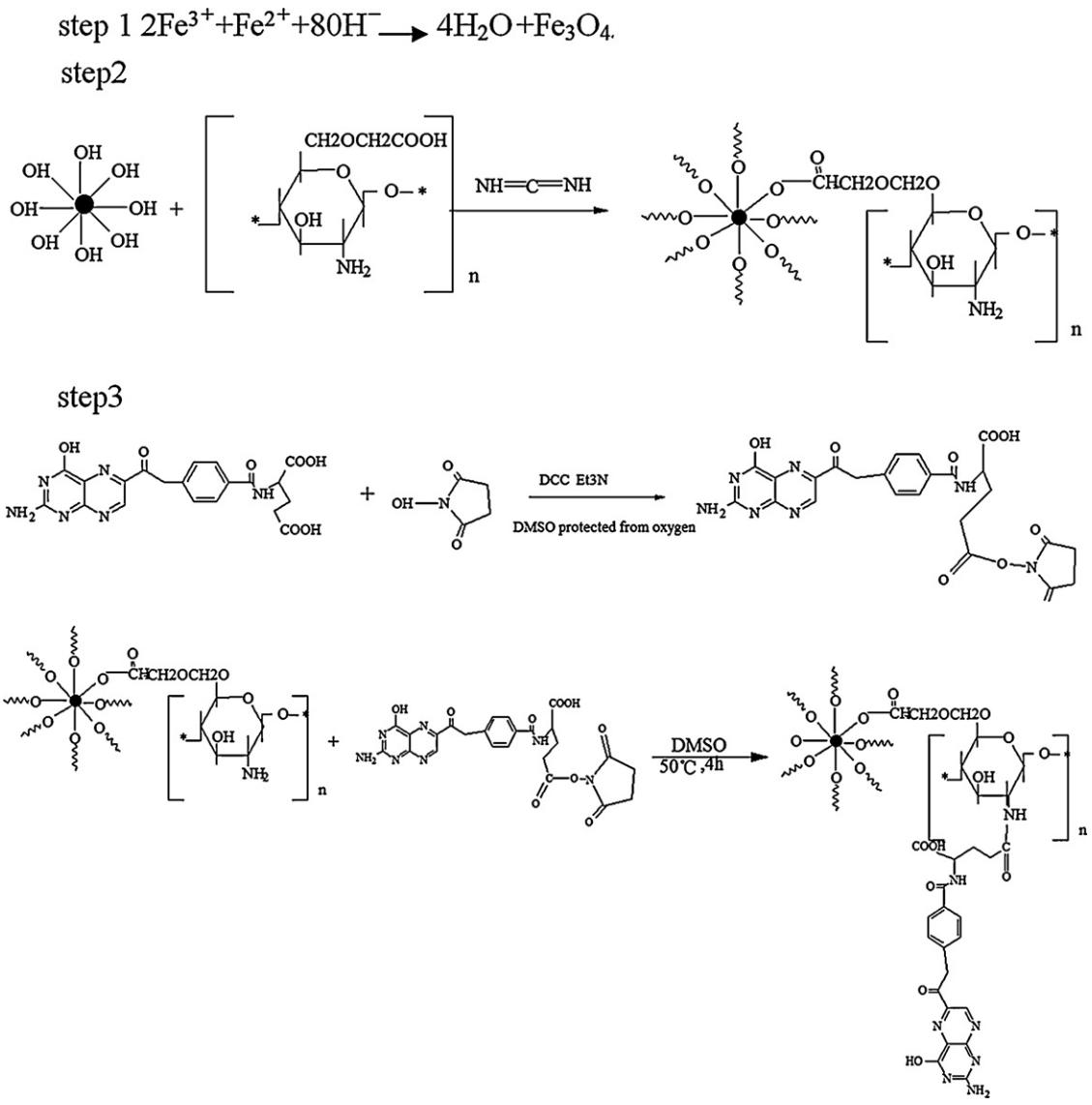

Fig. 1. Steps in the synthesis of folic acid(FA)-modified, *o*-carboxymethylchitosan (OCMCS)-coated magnetite nanoparticles.

ultrasonication for 10 min. Then, 10 ml of anhydrous DMSO solution containing 110 mg NHS-folate and 0.5 ml of triethylamine was added to the nanoparticles solution and continuously stirred for 4 h in a nitrogen atmosphere to form covalent bonding at the tethered amine sites on the OCMCS-SPIO-NPs; the folic acid-modified, OCMCS-encapsulated magnetic nanoparticles were then washed with ethanol and ultra pure water three times each and freeze-dried.

2.2.2. Preparation of dextran-coated SPIO nanoparticles

The dextran-coated SPIO nanoparticles, served as a control in this study, were prepared by alkaline co-precipitation of ferric chlorides ($FeC1_3{\cdot}6H_2O$), ferrous chlorides and dextran solution in anaerobic conditions at ambient temperature (Molday and MacKenzie, 1982).

2.3. Characterization

2.3.1. Fourier transform infrared spectroscopy

The functionalization of SPIO-NPs with OCMCS and folic acid was examined by Fourier transform infrared (FTIR) spectroscopy. FTIR spectra were acquired using an Analect RFX-65 Fourier transfer infrared spectrometer with a resolution of 4 cm^{-1}. FA-OCMCS-SPIO-NPs powder, OCMCS-SPIO-NPs powder, uncoated SPIO-NPs powder, pure OCMCS and folic acid were recorded with KBr discs in the range of 4000–400 cm^{-1}.

2.3.2. X-ray diffraction (XRD) measurement

The crystal structures of SPIO-NPs, OCMCS-SPIO-NPs and FA-OCMCS-SPIO-NPs were obtained by the powder XRD. Pattern of each sample was recorded with a D/Max-IIIA Powder X-ray Diffractometer using a monochromatized X-ray beam with nickel-filtered CuK_radiation with 4 min^{-1} scan rate. A continuous scan mode was used to collect 2θ data from 10° to 90°.

2.3.3. Transmission electron microscopy (TEM) measurement

The average particle size, size distribution and morphology of the samples were studied using a JEM-100CX II transmission electron microscope at a voltage of 200 kV. The composite dispersion was drop-cast onto a 200-mesh copper grid (Agar Scientific) and grid was air dried at room temperature before loading into the microscope. The size distribution was determined by measuring diameters of 100 particles in a TEM image.

2.3.4. Zata potential and hydrodynamic size

The Zata potential and hydrodynamic size of SPIO-NPs, OCMCS-SPIO-NPs, FA-OCMCS-SPIO -NPs and dextran-SPIO-NPs were determined in water by a dynamic laser light scattering (DLS) at a scattering angle of 90° at 25 °C using apparatus (MALVEN 3000HS ZETA SIZER, British). The suspension of nanoparticle prepared in water was used to measure zeta potential in phase analysis mode using the same apparatus.

2.3.5. Magnetic measurements

A VSM (MPMS XL-7 magnetometer) was used to characterize the magnetic properties of SPIO-NPs, OCMCS-SPIO-NPs and FA-OCMCS-SPIO-NPs. The hysteresis of the magnetization was obtained by changing outside fields (H) between +4000 and −4000 Oe. These measurements were carried out at 300 K.

2.3.6. Iron content in SPIO-NPs, OCMCS-SPIO-NPs and FA-OCMCS-SPIO-NPs

The iron content in the suspension and solid samples of uncoated-SPIO-NPs, OCMCS-SPIO-NPs and FA-OCMCS-SPIO-NPs was determined by *o*-phenanthroline method after 30% HCl acidation.

2.4. Cellular cytotoxicity and uptake

2.4.1. Cell culture

Both KB cells (a human oral epithelial cell line that over-express FR) and Hela cells (a human cervical cell line that moderately express FR) (positive control) were purchased from Keygen Biology and cultured in folate-free RPMI-1640 medium (FFRPMI1640). A549 cells (a human fibrosarcoma cell line lacking FR) (negative control) was a gift from Institute of Cancer Research of Nanfang Hospital and L-O2 cells (a human normal liver cell line) were purchased from Keygen Biologys. These two types of cells were cultured in full RPMI-1640 medium. RAW264.7 cells (a mouse monocyte–macrophage cell line), purchased from Keygen Biology were cultured in full high glucose Dulbecco Modified Eagle's Medium (DMEM, purchased from Keygen Biology). All the cells were routinely cultured at 37 °C in a humidified atmosphere with 5% CO_2 (in air).

2.4.2. Cell viability/cytotoxicity studies

To determine cell cytotoxicity/viability, KB, A549 and LO2 cells were seeded in 96-well tissue culture plates at a density of 5×10^3 cells/well in their respective culture full medium. After 24 h, the culture medium was replaced with 200 μl fresh medium containing 50–1000 μg/ml of nanoparticles (uncoated-SPIO-NPs, dextran-SPIO-NPs, OCMCS-SPIO-NPs or FA-OCMCS-SPIO-NPs, respectively). After another 24 h, the viability of the KB, A549 and LO2 cells was determined by tetrazolium dye (MTT) assay.

2.4.3. Visualization of the cellular uptake by Prussian blue staining

The cellular uptake of nanoparticles was visualized using Prussian blue staining via microscopy: All the cell lines were seeded onto the 6-well plate with 5×10^5 cells/well. After 24 h of incubation with their respective full culture medium, the supernatant was removed and cells were washed three times with PBS. 2 ml of the full DMEM culture medium containing SPIO-NPs, dextran-SPIO-NPs, OCMCS-SPIO-NPs or FA-OCMCS-SPIO-NPs (iron concentration of 0.4 mg/ml) was added to RAW264.7 cells respectively. While the full FFRPMI1640 medium containing OCMCS-SPIO-NPs (used as a negative contrast) or FA-OCMCS-SPIO-NPs (used as a positive sample) was added to KB, Hela and A549 cells at the same concentration, respectively. After incubation at 37 °C for 24 h, the supernatant was removed and cells were washed three times with PBS. Then the cells were treated with 0.5 M of 4% paraformaldehyde (PFA) solution for 10 min to fix the cells and washed with PBS. At last the cells were stained with Prussian blue (Chen et al., 2008). The wells without nanoparticles were used as blank. The Prussian blue staining results were assessed by a light microscope.

2.4.4. Quantification of cellular uptake by ferrozine assay

To quantitate intracellular uptake of the nanoparticles, cells were grown in 24-well culture plates with approximately 2.5×10^5 cells/well. After incubation at 37 °C for 24 h, the cells were washed three times with PBS. 1 ml of the full DMEM culture medium containing SPIO-NPs, dextran-SPIO-NPs, OCMCS-SPIO-NPs or FA-OCMCS-SPIO-NPs (iron concentration concentration ranging from 50 μg/ml to 800 μg/ml) was added to RAW264.7 cells respectively. While the full FFRPMI1640 medium containing OCMCS-SPIO-NPs (used as a negative contrast) or FA-OCMCS-SPIO-NPs (used as a positive sample) was added to KB, Hela and A549 cells at the same concentration, respectively. After 24 h of incubation with nanoparticles, iron content in each cell was measured using the ferrozine assay (Muller et al., 2007). Absorbance of samples were read at 490 nm using a BioRad microplate reader and concentrations calculated using a standard curve was prepared with ferrous ethylenediammonium sulfate in 0.01 N HCl ranging from 0 to 300 μmol/L.

2.5. Evaluation of the FR-tumor targeting in vivo

2.5.1. In vivo MR Imaging in nude mice

Animals (BACB/C-nu male nude mice scxk Yue 2006-0015) were purchased from the Southern Medical University Laboratory Animal Center, Guangzhou, Guangdong, China. Animal experiments were performed in accordance with the protocols approved by the University of Southern Medical University Committee on Use and Care of Animals. Animals were maintained on a folate-free diet for 6 weeks before MR imaging. Sixteen nude mice were divided into two groups equivalently: KB and A549 cells groups. Subcutaneous xenograft tumors were produced in animals by subcutaneous injection of 1×10^6 KB or A549 tumor cells in 100 μL of serum-free cell culture medium into the neck back respectively under anesthesia (chloral hydrate solution 400 mg/kg intraperitoneally). Animals were studied by MR imaging when the subcutaneous xenograft tumors reached a diameter of 1 cm. FA-OCMCS-SPIO-NPs (5.62 mg Fe/ml) or OCMCS-SPIO-NPs solution (5.54 mg Fe/ml) of 0.25 ml was infused intravenously into a nude mouse bearing the KB or A549 tumor. During imaging the mouse remained in the magnet and T_2-weighted gradient echo images were acquired before and after nanoparticles administration 2.5 h, using the following parameters: TR/TE 4000/85 ms; echo train length 26, bandwidth 15.63, flip 20°; FOV = 12 cm; slice thickness 3 mm.

2.5.2. Ex vivo histological analysis of xenograft tumors

Tumors were collected 3 h after injection of the contrast agent. Mice were deeply anesthetized with an intraperitoneal injection of chloral hydrate (400 mg/kg). The tumor tissues were excised and stored in 4% paraformaldehyde. Paraffin-embedded histological slices (3 mm thick) were stained with hematoxylin–eosin (H&E). Prussian blue staining was also used to identify the iron in the histological sections of the tumor. The samples were deparaffinized and rehydrated, then immersed in a solution containing 5% w/v of potassium ferrocyanide and 10% hydrochloric acid (v/v) in water for 3 h. Slides were rinsed with water and images obtained on a OLYMPUS DMR upright microscope (OLYMPUS Microsystems, Japan).

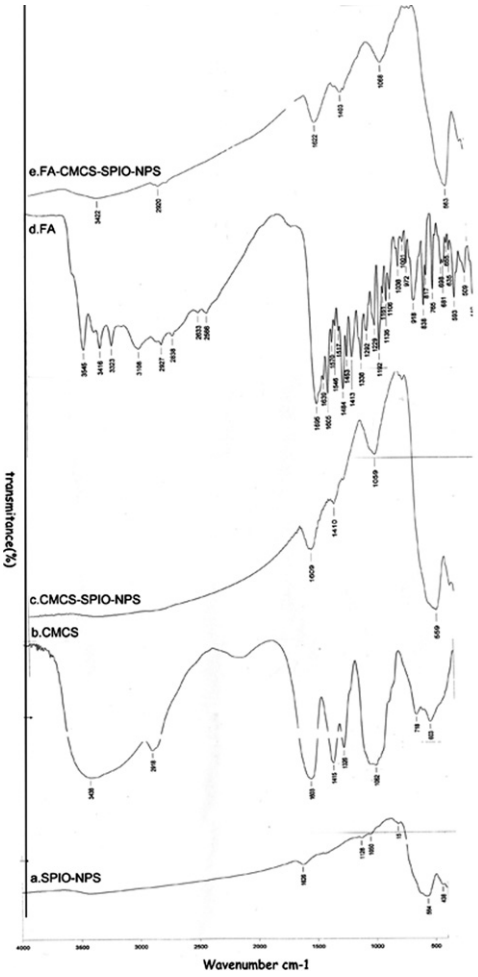

Fig. 2. Fourier transform infrared (FTIR) spectra of synthesized SPIO nanoparticles (a), OCMCS (b), OCMCS-coated SPIO nanoparticles (c), folic acid (pure) (d) and Folic acid-modified, OCMCS-coated SPIO nanoparticles (e).

2.6. Statistical analysis

Each experiment was repeated three times in duplicate. The statistical analysis of experimental data utilized the "compare means" in SPSS 13.0 statistical soft package and the results were presented as mean ± SD. Statistical significance was accepted at a level of $p < 0.05$.

3. Results

3.1. Surface characterization

3.1.1. FTIR spectra analysis

The FTIR spectra for naked SPIO-NPs (a), OCMCS (b), OCMCS-SPIO-NPs (c), folic acid (d) and FA-OCMCS-SPIO-NPs (e) were presented in Fig. 2. For the naked Fe_3O_4, Fig. 2a shows the peak of 564 cm^{-1}, which is typical characteristic of Fe–O–Fe in Fe_3O_4. However, from Fig. 2c and e, it can be seen that the characteristic peak of Fe–O–Fe shifted to 559 and 563 cm^{-1}, respectively. For the IR spectrum of OCMCS (Fig. 2b), the main characteristic absorption bands appeared at 1599 and 1411 cm^{-1}, which are attributed to the asymmetric and symmetric stretching vibration of COO, respectively. In the spectrum of OCMCS-SPIO-NPs (Fig. 2c), the 1599 and 1411 cm^{-1} peak of COO symmetric and asymmetric stretching vibration shifted to 1609 and 1410 cm^{-1}. The results indicate that OCMCS was bound to SPIO-NPs successfully. The FTIR spectra for pure folic acid and FA-OCMCS-SPIO-NPs were presented in Fig. 2d and e, Compared with FTIR spectra of pure folic acid, FTIR spectrum of FA-OCMCS-SPIO-NPs displays intense peaks at 1622 and 1403 cm^{-1} which might result from the aromatic ring stretch of the pteridine skeleton and p-amino benzoic acid moieties of folic acid. On the other hand, Fig. 2e displays two new characteristic absorption bands appeared at 3422 cm^{-1}, which might be due to the hydroxyl (OH) stretching and NH– stretching vibration bands of folic acid. Furthermore, the peak at 2920 cm^{-1} indicates that the –CH stretch of folic acid. These results confirm the SPIO-NPs, OCMCS-SPIO-NPs and FA-OCMCS-SPIO-NPs were successfully synthesized.

3.1.2. X-ray diffraction (XRD)

The XRD patterns for uncoated SPIO-NPs, OCMCS-SPIO-NPs and FA-OCMCS-SPIO-NPs were shown in Fig. 3a–c, respectively. Six characteristic peaks for Fe_3O_4 ($2\theta = 30.1^\circ$, 35.5°, 43.1°, 53.4°, 57.0°, and 62.6°) marked by their indices ((2 2 0), (3 1 1), (4 0 0), (4 2 2), (5 1 1), and (4 4 0)) were observed in all of the samples, Which was in good agreement with that of standard Fe_3O_4 spinal structure (Santra et al., 2001). These results indicate that the SPIO-NPs were pure Fe_3O_4, furthermore, the functionalization of the folic acid and OCMCS had no influence on the crystal phase of Fe_3O_4.

3.1.3. TEM morphology

Transmission electron microscopy (TEM) micrographs of magnetite nanoparticles were presented in Fig. 4. It can be seen from Fig. 4a–c that all the synthesized uncoated SPIO-NPs, OCMCS-SPIO-NPs and FA-OCMCS-SPIO-NPs were almost spherical or ellipsoidal. The mean particle size and standard deviation were 12.5 nm and 3.0 nm for uncoated SPIO-NPs, 13.7 and 3.6 nm for OCMCS-SPIO-NPs, 15.4 nm and 4.5 nm for FA-OCMCS-SPIO-NPs, respectively.

3.1.4. Zeta potential and hydrodynamic size

The mean hydrodynamic diameter measured by DLS was 38.2 nm with a polydispersity index of 0.119 for OCMCS-SPIO-NPs, 41.4 nm with a polydispersity index of 0.132 for FA-OCMCS-SPIO-NPs, and 125 nm with a polydispersity index of 0.143 for dextran-SPIO-NPs. However, the mean particle radius for unmodified magnetic nanoparticles showed 201 nm with a polydispersity index of 0.245, which might be due to a very fast and strong flocculation without the material coated the SPIO-NPs. The zeta potential of suspension for OCMCS-SPIO-NPs and FA-OCMCS-SPIO-NPs were -21.36 ± 1.15 mV and -27.88 ± 0.73 mV, respectively. These results demonstrated that the hydrodynamic size of OCMCS-SPIO-NPs and FA-OCMCS-SPIO-NPs were smaller than that of dextran-SPIO and SPIO nanoparticles, along with the strong zeta potential to keep the solution from aggregation.

3.1.5. Magnetic results

Magnetization hysteresis loops at 300 K of uncoated, OCMCS-coated and folic acid-modified OCMCS-coated SPIO nanoparticles (Fig. 5) demonstrate that all the three SPIO-NPs show superparamagnetic property. The specific saturation magnetism σ_s for the uncoated SPIO, OCMCS-SPIO and FA-OCMCS-SPIO nanoparticles were 98.05, 71.4 and 69.6 emu/g Fe, respectively. We can observe from Fig. 5 that σ_s decreased after the particles coated. The decrease of the magnetization might be due to the coating polymer on the magnetic nanoparticles.

3.2. Cellular uptake and cytotoxicity of nanoparticles

3.2.1. Nanoparticles cytotoxicity

Fig. 6 demonstrateed that dose-dependent reductions in viability of all three cells (LO2, A549 and KB cells)treated with uncoated

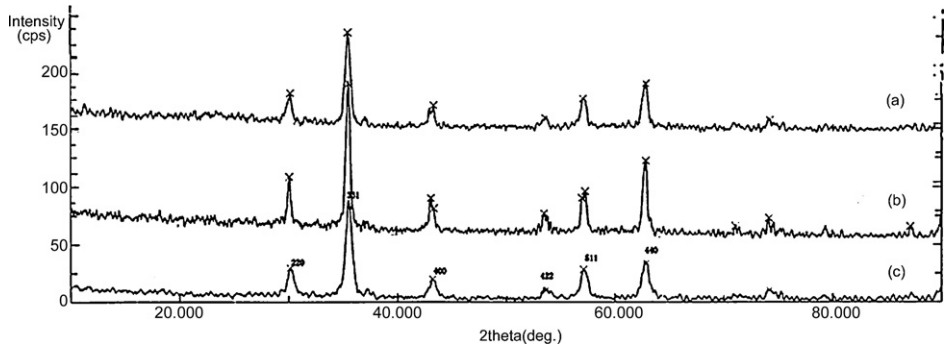

Fig. 3. XRD patterns for the uncoated-SPIO nanoparticles (a), OCMCS-SPIO nanoparticles (b) and FA-OCMCS-SPIO nanoparticles(c).

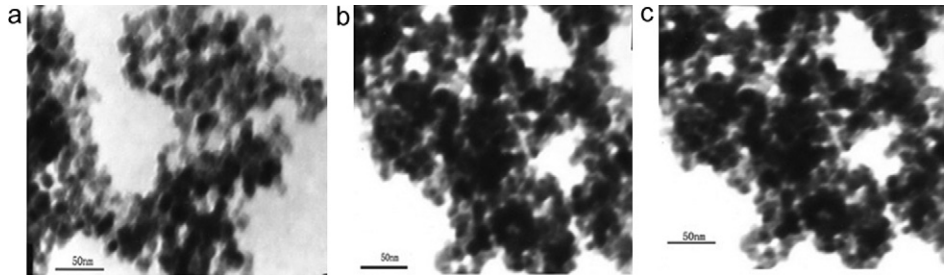

Fig. 4. TEM images of uncoated-SPIO-NPs (a), OCMCS-SPIO-NPs (b) and FA-OCMCS-SPIO-NPs (c) (Bar = 50 nm).

SPIO-NPs, OCMCS-SPIO-NPs, FA-CMCS-SPIO-NPs or dextran-SPIO-NPs respectively for 24 h. Uncoated SPIO-NPs caused a significant reduction ($60.0 \pm 6.4\%$, $58.7 \pm 5.6\%$ and $33.3 \pm 3.4\%$, respectively of control) in the viability of LO2, A549 and KB cells until the iron concentration reached 200 μg/ml, and induced further reductions at higher concentrations; the viability of LO2, A549 and KB cells were $7.41 \pm 3.32\%$, $9.98 \pm 7.01\%$ and $1.52 \pm 0.553\%$, respectively, when the iron concentration came to 1000 μg/ml. After 24 h of incubation with OCMCS-SPIO-NPs or FA-OCMCS-SPIO-NPs, only slight cytotoxicity was observed, and the survival rate of all three cells was higher than 70% even at the highest nanoparticles concentration (iron concentration was up to1000 μg/ml). There was no significant difference between the cytotoxicity of OCMCS-SPIO-NPs and dextran-SPIO-NPs against LO2, A549 cells. Furthermore, folic acid further modifying significantly increased the cytotoxicity of nanoparticles against KB cells, while, it had no influence on their cytotoxicity against the A549 cells.

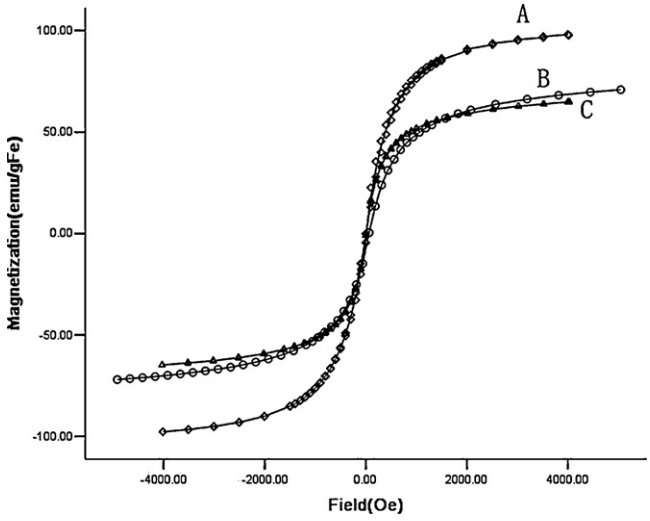

Fig. 5. Magnetization curve for the uncoated-SPIO-NPs (A), OCMCS-SPIO-NPs (B) and FA-OCMCS-SPIO-NPs(C) at 300 K.

3.2.2. Uptake of the nanoparticles by mouse macrophage

The Prussian blue staining images of mouse macrophage after cultured in the medium containing the uncoated SPIO-NPs, OCMCS-SPIO-NPs, dextran-SPIO-NPs and FA-OCMCS-SPIO-NPs are showed in Fig. 7. The color of cells through Prussian blue staining suggested the cellular uptake of nanoparticles. In Fig. 7, images from weak to dark were as following: blank, FA-OCMCS-SPIO-NPs, OCMCS-SPIO-NPs, dextran-SPIO-NPs and SPIO-NPs. The result indicated that the modification with OCMCS alone or OCMCS and folic acid simultaneously could dramatically decrease the internalization of the nanoparticles by mouse macrophage cells, and the intercellular iron content of RAW264.7 cells cultured with OCMCS-SPIO-NPs or FA-OCMCS-SPIO-NPs was even lower than that cultured with dextran-SPIO-NPs.

The cellular uptake of nanoparticles by mouse macrophage cells was quantified by ferroine assay after the cells were grown in medium containing uncoated SPIO-NPs, dextran-SPIO-NPs, OCMCS-SPIO-NPs and FA-OCMCS-SPIO-NPs. Fig. 8 demonstrates a dose-dependent increase in intracellular iron content for cells treated with SPIO-NPs (concentration range 50–800 μg/ml) for 24 h, the intracellular iron content increased with the increase of iron concentration ranging from 50 to 200 μg/ml. At higher concentration, the intracellular iron content reached to plateau around 200 μg/ml, then, at the highest concentration (800 μg/ml), the intracellular iron content came to 88.39 ± 1.18 pg/cell. After OCMCS coating or folic acid modification and OCMCS coating, the uptake of nanoparticles by mouse macrophage cells decreased greatly. The average uptake of OCMCS-SPIO-NPs and FA-OCMCS-SPIO-NPs by mouse macrophage cells was 6.96 and 5.64 pg/cell, respectively, which was less than that of dextran-SPIO-NPs (8.61 pg/cell), even far less than that of uncoated SPIO-NPs (75.67 pg/cell). The experimental results showed that there was almost no significant difference in cellular uptake of nanoparticles by mouse macrophage cells after folic acid modification.

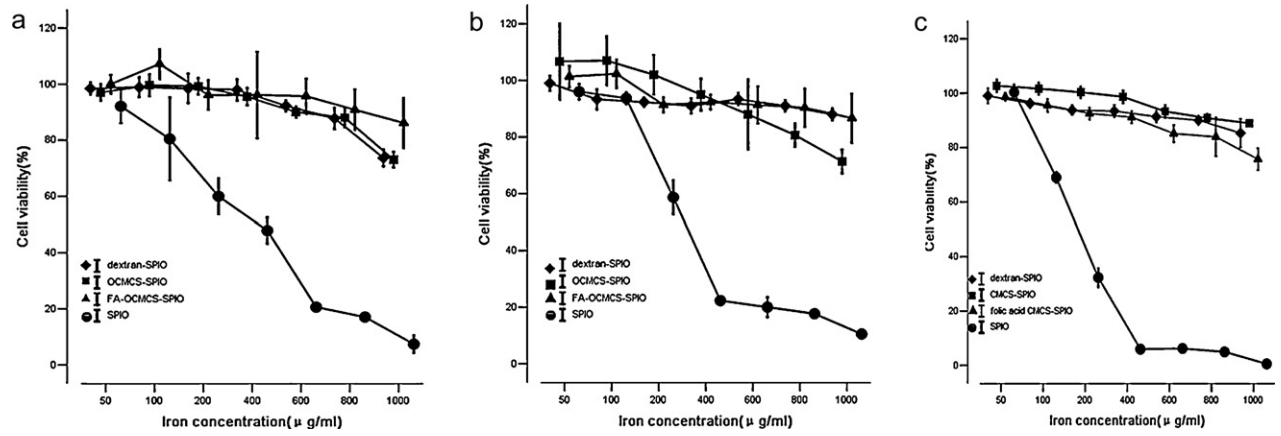

Fig. 6. Viability of uncoated SPION-NPs, OCMCS-SPIO-NPs, FA-OCMCS-SPIO-NPs and dextran-SPIO-NPs at various iron concentrations ranging from 50 to 1000 μg/mL, when incubated with LO2 (a), A549 (b) and KB(c) cells determined by MTT assay. Percent viability of cells was expressed relative to control cells. Results are represented as mean ± SD.

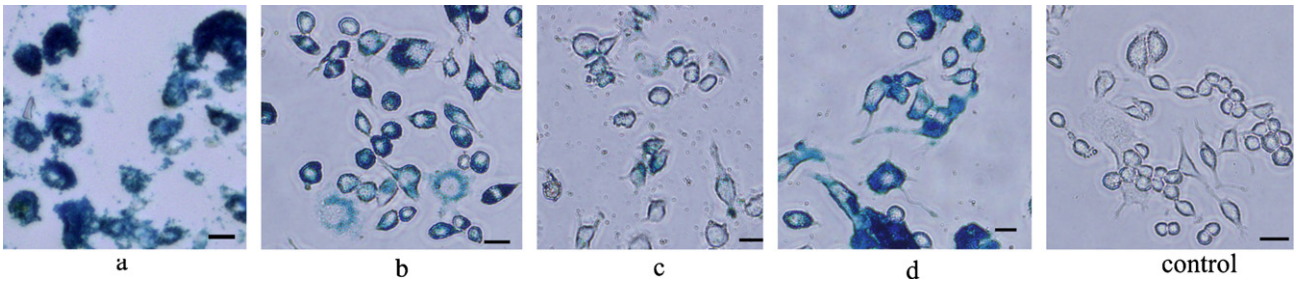

Fig. 7. Prussian blue staining micrographs of macrophage cells (RAW264.7 cells) treated with uncoated-SPIO-NPs (a), OCMCS- SPIO-NPs (b), FA-OCMCS-SPIO-NPs(c) and dextran- SPIO-NPs (d) (control, without contrast agent). (For interpretation of the references to color in this figure legend, the reader is referred to the web version of the article.)

3.2.3. *Uptake of the nanoparticles by three cancer cells*

The FR mediated cell targeting was confirmed by Prussian blue staining study *in vitro*. Fig. 9 shows the FR-positive cells (Hela or KB cells) incubated with FA-OCMCS-SPIO-NPs (400 μg/ml) had massive positive staining, while the same cells incubated with the same amount of OCMS-SPIO-NPs resulted in almost no particles-cluster. Furthermore, there was little difference on positive staining of A549 cells incubated with FA-OCMCS-SPIO and OCMCS-SPIO nanoparticles.

The results assessed by ferrozine assay are presented in Fig. 10a–c. Fig. 10 indicated that, at first, the iron content in each cell increased with the iron concentration and then reached to a plateau for both OCMCS-SPIO-NPs and FA-OCMCS-SPIO-NPs. Folic acid modification could dramatically improve the uptake of nanoparticles by Hela and KB cells, while had little influence on the uptake of nanoparticles by A549 cells, the improvement had correlation relation with the amount of FR on the surface of cancer cells.

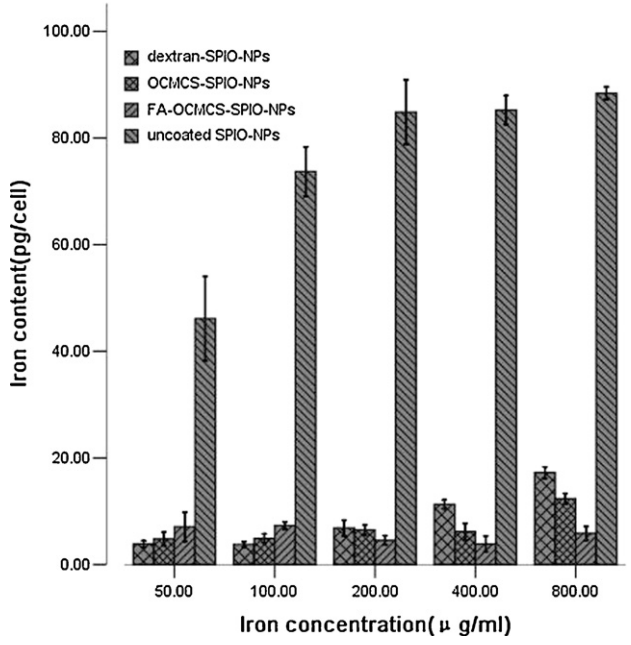

Fig. 8. Histogram of intracellular iron content of RAW264.7 cells after treated with uncoated-SPIO-NPs, dextran-SPIO-NPs, OCMCS-SPIO-NPs or FA-OCMCS-SPIO-NPs (the iron concentration in culture medium ranging from 50 to 800 μg/ml) Three sets of duplicates were performed for each data point.

3.3. *FR-targeting in vivo*

3.3.1. *Magnetic resonance imaging in vivo*

Fig. 11a–d shows the T2-weighted spin echo images of the tumor-bearing mice, acquired before and 2.5 h after intravenous administration of the OCMCS-SPIO or FA-OCMCS-SPIO nanoparticles, respectively. The signal intensity changed from region of interest is showed in Table 1. Region of interest over the entire KB cells subcutaneous tumors indicate that the average intensity decreases about 27.23% between preinjection and postinjection images for FA-OCMCS-SPIO-NPs ($p = 0.01 < 0.05$). However, the signal intensity had no significant drop between preinjection and postinjection images of subcutaneous tumors for other groups ($p > 0.05$). Here we demonstrated that the FA-OCMCS-SPIO-NPs only accumulated in the tumor that over express folate receptor.

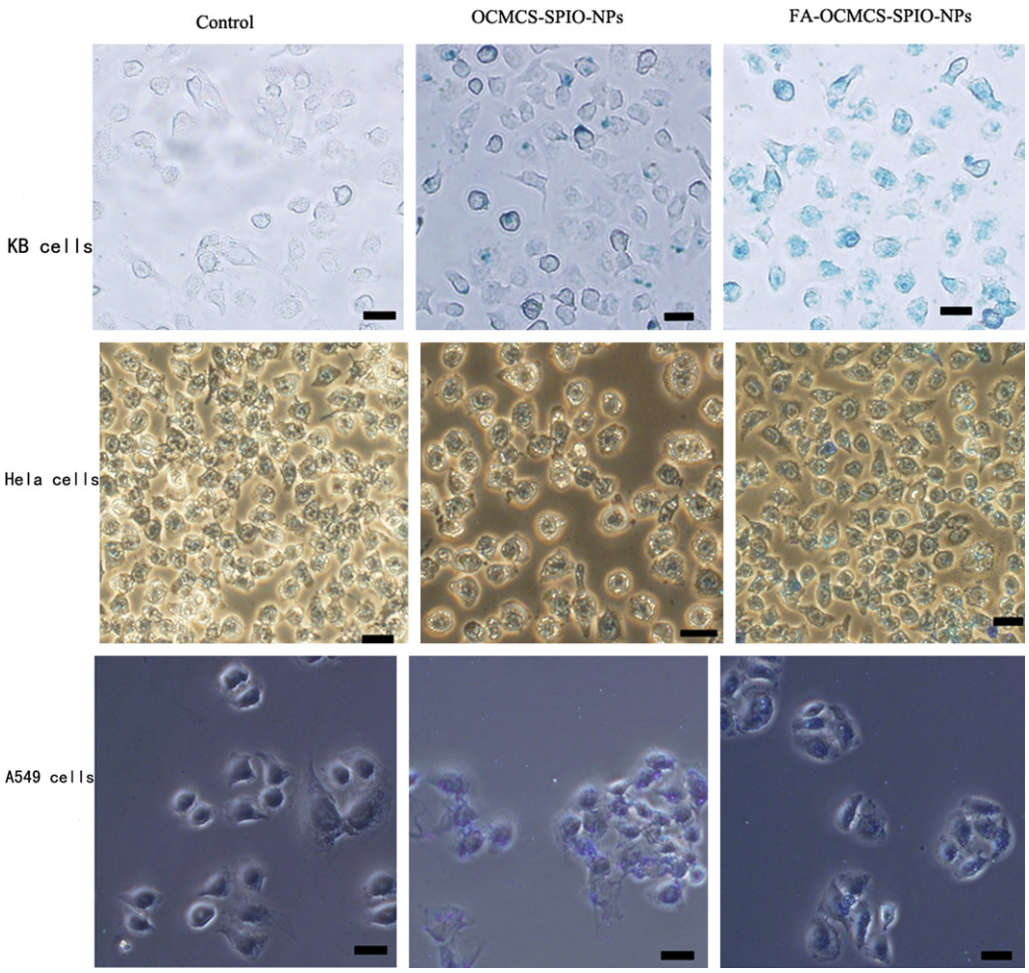

Fig. 9. Prussian blue staining images of KB, Hela and A549 cells after treated with OCMCS- SPIO-NPs or FA-OCMCS- SPIO-NPs, respectively (control, untreated with SPIO-NPs). (For interpretation of the references to color in this figure legend, the reader is referred to the web version of the article.)

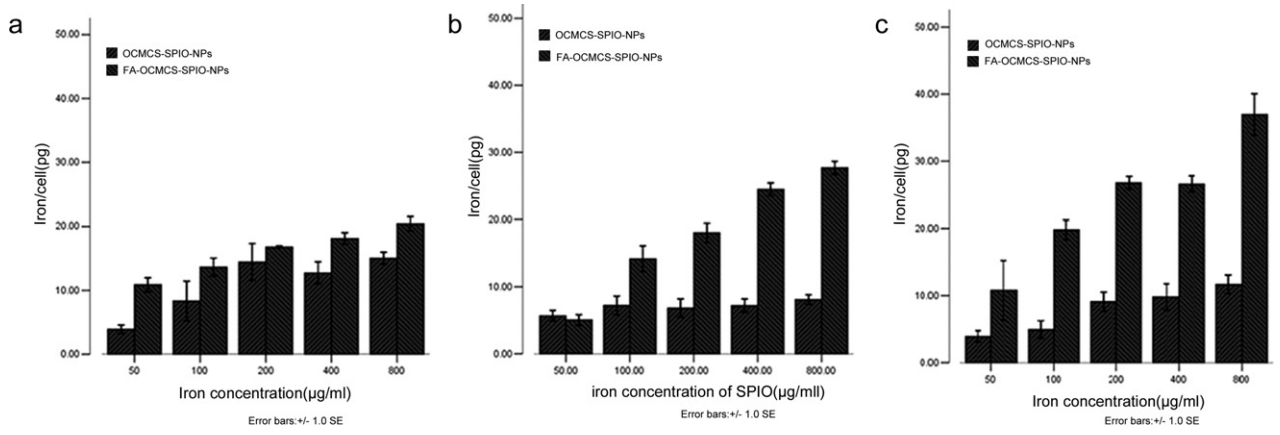

Fig. 10. Histogram of intracellular iron content of A549 cells (a), Hela cells (b) and KB cells (c) cultured in medium containing OCMCS-SPIO-NPs or FA-OCMCS-SPIO-NPs with different concentration determined by ferroine assay. Three sets of duplicates were performed for each data point. Results are represented as mean ± SD.

Table 1
MRI signal intensity of KB or A549 xenografts tumors change from OCMCS-SPIO-NPs or FA-OCMCS-SPIO-NPs.

	Preinjection	Postinjection	Change	*p*	Preinjection	Postinjection	Change	*p*
A549 cell xenografts tumors	699.90 ± 45.60	698.24 ± 47.68	0.24%	0.722	747.64 ± 31.67	748.58 ± 38.67	−0.13%	0.367
KB cell xenografts tumors	648.00 ± 18.29	639.87 ± 26.75	1.25%	0.367	602.36 ± 10.30	438.34 ± 14.81	27.23%	0.01*

The statistical analysis of experimental data utilized the "paired-samples t test SPSS.13 statistical soft package. Intensity is presented as mean ± standard deviation. Percent change of intensity is calculated as (post − pre)/pre × 100%.

* $p < 0.05$.

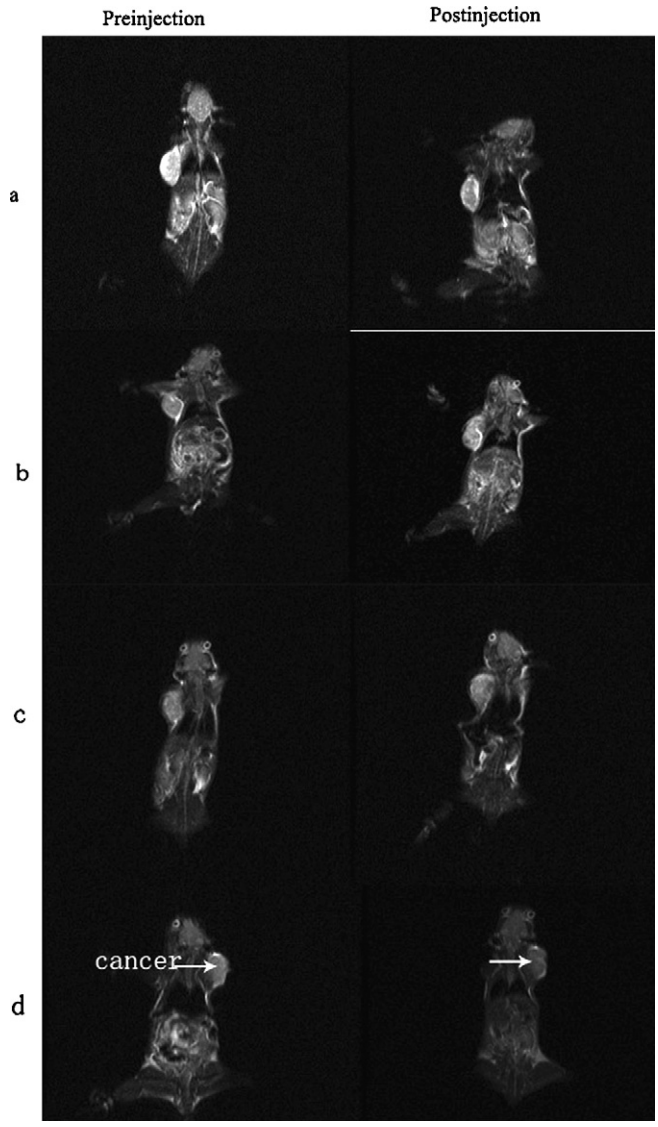

Fig. 11. T2 weight imaging of tumor-bearing mice injected with FA-OCMCS-SPIO-NPs or OCMCS-SPIO-NPs: A549 tumor-bearing mice injected with OCMCS-SPIO-NPs (a) or FA-OCMCS-SPIO-NPs(b) and KB tumor-bearing mice injected with OCMCS-SPIO-NPs (c) or FA-OCMCS-SPIO-NPs (d). (For interpretation of the references to color in this figure legend, the reader is referred to the web version of the article.)

3.3.2. Histology

H&E stained image (Fig. 12) demonstrates that only in KB tumor tissues slice from mice intravenously injection with FA-OCMCS-SPIO-NPs, black SPIO-NPs clusters could be seen, on the contrary, no black SPIO-NPs cluster was evident in other H&E stained images. At the same time, In Fig. 13, very strong blue color can be seen in the KB tumor tissue after tumor-bearing mice were intravenously injection with FA-OCMCS-SPIO-NPs, but no blue color staining was showed in other images, which were coincided with the results from H&E stained image. All these results further confirmed the FR tumor-specific uptake of FA-OCMCS-SPIO-NPs after systemic administration.

4. Discussion

The surface properties of SPIO-NPs play a critical role in determining the physicochemical property as well as the interactions of SPIO-NPs with proteins, cells, and tumor tissues (Berry et al., 2004). Our results demonstrated that the OCMCS covalently conjugated to SPIO-NPs significantly increased the colloid stability and hydrophilic property of SPIO-NPs, dramatically reduced the capture by mouse macrophage cells, and significantly decreased the cytotoxicity. According to FTIR results, OCMCS with functional carboxyl groups is bound on the surface of Fe_3O_4 by the covalent bonds of "O" of hydrous Fe_3O_4 and "C=O" of carboxyl groups in OCMCS molecules. The carboxyl groups render the modified SPIO-NPs negatively charged, thereby preventing particles from agglomerating by the electrostatic repulsion. At the same time, the OCMCS's modification can increase the surface hydrophilicity, minimizing adherence to cell membranes by hydrophobic interaction, the first step required for phagocytosis. The small hydrophilic size (<50 nm) of OCMCS-SPIO-NPs and their hydrophilic surface could significantly improve the stabilization of the suspension, reduce the protein absorption and increase the surface hydrophilicity of SPIO-NPs, thus avoiding their recognition and capturing by mouse macrophage cells, On the contrary, the hydrophobic uncoated-SPIO-NPs can be readily taken up by the mouse macrophage cells through endocytosis. As evidence, the iron content in RAW264.7 cells cultured in OCMCS-SPIO-NPs or FA-OCMCS-SPIO-NPs was much lower than in the cells that were exposed to dextran-SPIO-NPs suspension. Furthermore, modification with folic acid posed little impact on the mouse macrophage capture, presumably due to the nature of folic acid as a low molecular weak acid and its insignificant impact on the particle sizes and surface charge (Zhang et al., 2002).

The dose-dependent cytotoxicity of four kinds of SPIO-NPs against the three cells (LO2, A549 and KB cells) was similar to other reports on cytotoxicity of dextran stabilized SPIO-NPs in culture. Human dermal fibroblasts incubated with dextran stabilized SPIO-NPs increase cell death and apoptosis after 48 h at a concentration of 0.05 mg/ml (Berry et al., 2004). Ferumoxides resulted in significant apoptosis in human monocytes after 4 h at concentrations of 0.5 g/ml and above (Metz et al., 2004). Our results demonstrated that the OCMCS covalently conjugated to SPIO-NPs induced distinct reduction in cytotoxicity. Interestingly the folic acid modification only increased the nano-cytotoxicity against the FR over-expressed KB cells, while had little adverse impact on the FR negatively expressed A549 cells. This is probably due to the modification of FA promoting the FA-OCMCS-SPIO-NPs uptake by KB cells and leading to a major increase in nanoparticles accumulation in the KB cells. The mechanism for SPIO-NPs cytotoxicity, when it does occur, has been proposed as responding to reactive oxygen species (ROS) production via Fenton or Haber–Weiss reactions, which is caused by the release of free iron ions and can result in lipid peroxidation, DNA damage, and protein oxidation (Lewinski et al., 2008).

The folic acid modification was shown to possess the ability to significantly improve the specific tumor cell target *in vitro* and *in vivo*. *In vitro* studies indicated that the FR tumor target was correlated with the amount of FR on cellular surface. This coincided with the results from the FA-PEG-modified SPIO-NPs (Zhang et al., 2002), accounting for the FR mediated endocytosis—the mainly mechanisms for the tumor-cellular internalization of folic acid (Low and Antony, 2004). It indicated that cellular uptake efficiency is largely dependent on both the amount of the FR on the surface of the tumor cells and the folic acid/folic acid polymer that reach the surface of the cells.

The further folic acid conjugation could also enhance the efficiency and specificity of OCMCS-SPIO-NPs for hyperthermia. During the hyperthermia, an alternating magnetic field can be applied to tumor cells containing SPIO-NPs to heat and selectively kill cancer cells, which are more sensitive to high temperature than healthy cells (Hou et al., 2009). On the other hand, FA-OCMCS-SPIO-NPs could also be used as potential drug delivery carrier by conjugating with small drugs, polypeptides, genes, antibodies, proteins and protein toxins. The nanoparticles could localize

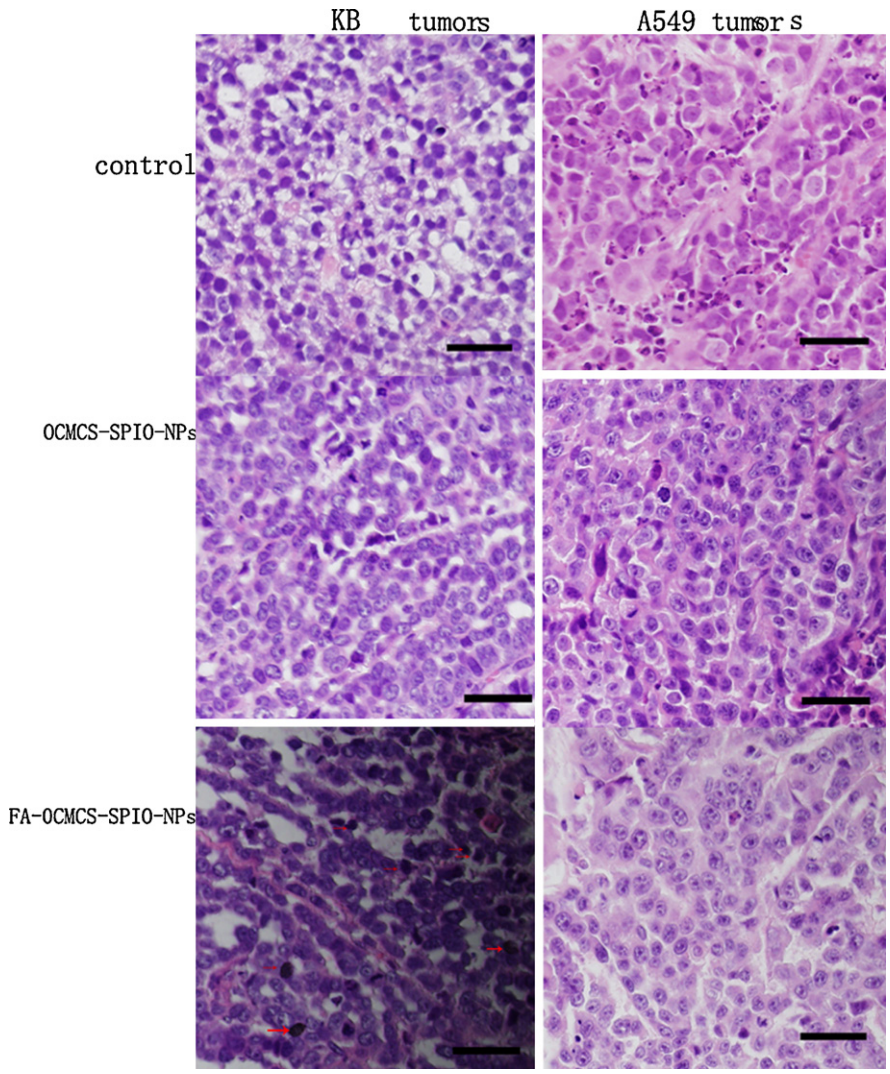

Fig. 12. H&E staining micrograph of KB or A549 cells subcutaneous tumor tissues after the mice were intravenously (via the tail vein) injected with the CMCS-SPIO-NPs or FA-CMCS-SPIO-NPs, respectively. The tumor tissue of the mice were not injected any nanoparticles were used as control (the scale bars are 50 μm). (For interpretation of the references to color in this figure legend, the reader is referred to the web version of the article.)

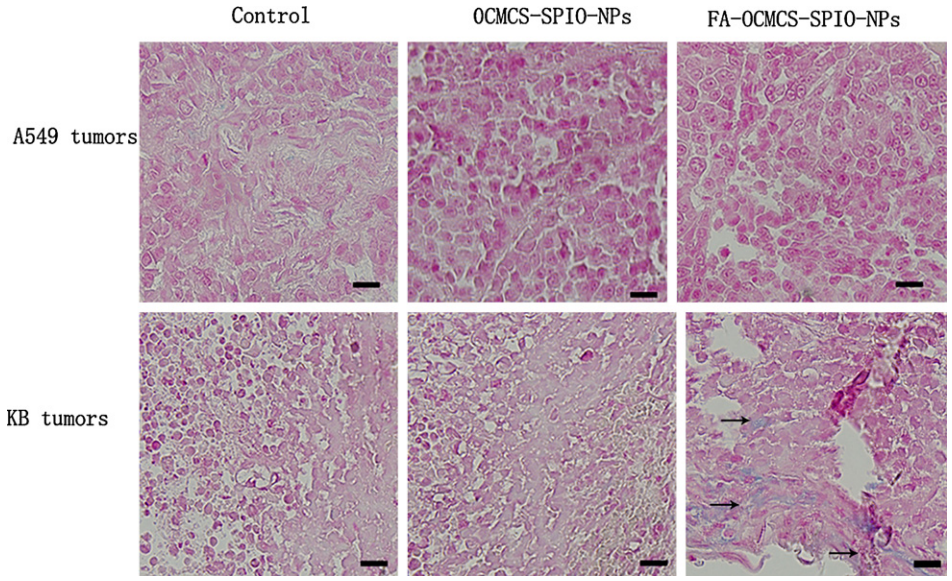

Fig. 13. Prussian blue staining micrographs of KB or A549 cells subcutaneous tumor tissues after the mice were intravenously (via the tail vein) injected with the CMCS-SPIO-NPs or FA-CMCS-SPIO-NPs, respectively, The tumor tissue the mice were not injected any nanoparticles were used as control (the scale bars are 25 μm). (For interpretation of the references to color in this figure legend, the reader is referred to the web version of the article.)

to an area of interest via a receptor-mediated endocytosis or by an external magnetic field. Importantly, it was reported that folate–macromolecule conjugates would not rapidly degrade following internalization by FR-mediated endocytic process. As a result, the delivery systems could potentially develop for the hydrolytically sensitive macromolecules, e.g., proteins and gene therapy vectors (Lu and Low, 2002; Low and Antony, 2004). These properties indicated the promise of FA-OCMCS-SPIO-NPs in drug delivery system for not only small drugs but also macromolecule drugs, furthermore, the FA-OCMCS-SPIO-NPs drug delivery system with both real-time imaging and drug delivery capabilities are of clinical importance as it could allow simultaneous detection of pathologies as well as delivery of therapeutics.

In vitro and *in vivo* studies also illustrated that the folic acid-modification can neither increase the uptake of FA-OCMCS-SPIO-NPs by A549 nor increase the MRI signal intensity of A549 subcutaneous tumors. A possible explanation was that, the cellular uptake of FA-OCMCS-SPIO-NPs by negatively FR-expressed A549 cells did not benefit from the FR modification. Since not all cancer cell lines over express FR, the nanoparticles will be able to be modified with other alternative tumor-specific ligands in order to realize specific drug delivery and MRI imaging for tumors without FR overexpression, such as prostate, bladder, and lymphoid cancers.

5. Conclusions

In conclusion, the FA-OCMCS-SPIO-NPs with hydrophilic size about 35–50 nm have successfully prepared. The results demonstrated that the FA-OCMCS-SPIO-NPs were of hydrophilicity, low macrophage uptake, low cytotoxicity, and excellent stability under the physiological condition. Moreover, FA-OCMCS-SPIO-NPs achieved an efficient FR tumor-target *in vivo*. The modification of SPIO- NPs with folic acid and OCMCS is a promising method to improve the stability and specific FR tumor-target of SPIO-NPs, thus boosting the application of SPIO-NPs in MRI imaging, drug delivery and hyperthermia.

Acknowledgements

The authors would like to thank the Center of Clinical Trials of Nanfang Hospital, Southern Medical University for providing the cell culture facilities.

References

Agnihotri, S.A., Mallikarjuna, N.N., Aminabhavi, T.M., 2004. Recent advances on chitosan-based micro- and nanoparticles in drug delivery. J. Control Release 100, 5–28.

Berry, C.C., Well, S., Charles, S., et al., 2004. Cell response to dextranderivatised iron oxide nanoparticles post internalization. Biomaterials 25, 5405–5413.

Chen, T.J., Cheng, T.H., Hung, Y.C., Lin, K.T., Liu, G.C., Wang, Y.M., 2008. Targeted folic acid-PEG nanoparticles for noninvasive imaging of folate receptor by MRI. J. Biomed. Mater. Res. A 87, 165–175.

Choi, H., Choi, S.R., Zhou, R., Kung, H.F., Chen, I.W., 2004. Iron oxide nanoparticles as magnetic resonance contrast agent for tumor imaging via folate receptor-targeted delivery. Acad. Radiol. 11, 996–1004.

Corot, C., Robert, P., Idee, J.M., Port, M., 2006. Recent advances in iron oxide nanocrystal technology for medical imaging. Adv. Drug Deliv. Rev. 58, 1471–1504.

Elsabee, M.Z., Morsi, R.E., Al-Sabagh, A.M., 2009. Surface active properties of chitosan and its derivatives. Colloids Surf. B Bio. Interfaces 74, 1–16.

Gnanaprakash, G., Mahadevan, S., Jayakumar, T., Kalyanasundaram, P., Philip, J., Raj, B., 2007. Effect of initial pH and temperature of iron salt solutions on formation of magnetite nanoparticles. Mater. Chem. Phys. 103, 168–175.

Gupta, A.K., Gupta, M., 2005. Synthesis and surface engineering of iron oxide nanoparticles for biomedical applications. Biomaterials 26, 3995–4021.

Heymer, A., Haddad, D., Weber, M., Gbureck, U., Jakob, P.M., Eulert, J., et al., 2008. Iron oxide labelling of human mesenchymal stem cells in collagen hydrogels for articular cartilage repair. Biomaterials 29, 1473–1483.

Hou, C.H., Hou, S.M., Hsueh, Y.S., et al., 2009. The in vivo performance of biomagnetic hydroxyapatite nanoparticles in cancer hyperthermia therapy. Biomaterials 30, 3956–3960.

Ito, A., Shinkai, M., Honda, H., Kobayashi, T., 2005. Medical application of functionalized magnetic nanoparticles. J. Biosci. Bioeng. 100, 1–11.

Katas, H., Alpar, H.O., 2006. Development and characterisation of chitosan nanoparticles for siRNA delivery. J. Control Release 115, 216–225.

Leamon, C.P., Low, P.S., 2001. Folate-mediated targeting: from diagnostics to drug and gene delivery. Drug Discov. Today 6, 44–51.

Lewinski, N., Colvin, V., Drezek, R., 2008. Cytotoxicity of nanoparticles. Small 4, 26–49.

Low, P.S., Antony, A.C., 2004. Folate receptor-targeted drugs for cancer and inflammatory diseases. Adv. Drug Deliv. Rev. 56, 1055–1058.

Lu, Y., Low, P.S., 2002. Folate-mediated delivery of macromolecular anticancer therapeutic agents. Adv. Drug Deliv. Rev. 54, 675–693.

Metz, S., Bonaterra, G., Rudelius, M., et al., 2004. Capacity of human monocytes to phagocytose approved iron oxide MR contrast agents in vitro. Euro. Radiol. 14, 1851–1858.

Molday, R.S., MacKenzie, D., 1982. Immunospecific ferromagnetic iron-dextran reagents for the labeling and magnetic separation of cells. J. Immunol. Methods 52, 353–367.

Muller, K., Skepper, J.N., Posfai, M., Trivedi, R., Howarth, S., Corot, C., et al., 2007. Effect of ultrasmall superparamagnetic iron oxide nanoparticles (Ferumoxtran-10) on human monocyte-macrophages in vitro. Biomaterials 28, 1629–1642.

Parker, N., Turk, M.J., Westrick, E., Lewis, J.D., Low, P.S., Leamon, C.P., 2005. Folate receptor expression in carcinomas and normal tissues determined by a quantitative radioligand binding assay. Anal. Biochem. 338, 284–293.

Reddy, J.A., Low, P.S., 1998. Folate-mediated targeting of therapeutic and imaging agents to cancers. Crit. Rev. Ther. Drug Carrier Syst. 15, 587–627.

Santra, S., Tapec, R., Theodoropoulou, N., Donson, J., Hebard, A., Tan, W.H., 2001. Synthesis and characterization silica-coated iron oxide nanoparticles in microemulsion. The effect of nonionic surfactants. Langmuir 17, 2900–2906.

Shubayev, V.I., Pisanic, T.R., Jin, S., 2009. Magnetic nanoparticles for theragnostics. Adv. Drug Deliv. Rev. 61, 467–477.

Stella, B., Arpicco, S., Peracchia, M.T., Desmaele, D., Hoebeke, J., Renoir, M., et al., 2000. Design of folic acid-conjugated nanoparticles for drug targeting. J. Pharm. Sci. 89, 1452–1464.

Sudimack, J., Lee, R.J., 2000. Targeted drug delivery via the folate receptor. Adv. Drug Deliv. Rev. 41, 147–162.

Sun, C., Sze, R., Zhang, M., 2006. Folic acid-PEG conjugated superparamagnetic nanoparticles for targeted cellular uptake and detection by MRI. J. Biomed. Mater. Res. A 78, 550–557.

Sun, C., Lee, J.S., Zhang, M., 2008. Magnetic nanoparticles in MR imaging and drug delivery. Adv. Drug Deliv. Rev. 60, 1252–1265.

Veiseh, O., Gunn, J.W., Zhang, M., 2010. Design and fabrication of magnetic nanoparticles for targeted drug delivery and imaging. Adv. Drug Deliv. Rev. 62, 284–304.

Zhang, Y., Kohler, N., Zhang, M., 2002. Surface modification of superparamagnetic magnetite nanoparticles and their intracellular uptake. Biomaterials 23, 1553–1561.

Zhou, L., Wang, Y., Liu, Z., Huang, Q., 2006. Carboxymethyl chitosan–Fe_3O_4 nanoparticles: preparation and adsorption behavior toward Zn^{2+} ions. Acta Phys. Chim. Sin. 22, 1342–1346.

Zhu, A., Jin, W., Yuan, L., et al., 2007. *O*-Carboxymethylchitosan-based novel gatifloxacin delivery system. Carbohyd. Polym. 68, 693–700.

Zhu, A., Yuan, L., Liao, T., 2008. Suspension of Fe_3O_4 nanoparticles stabilized by chitosan and o-carboxymethylchitosan. Int. J. Pharm. 350, 361–368.